Applied Catalysis B: Environmental 236 (2018) 233–239

Contents lists available at ScienceDirect

Applied Catalysis B: Environmental

journal homepage: www.elsevier.com/locate/apcatb

Rational design and facile in situ coupling non-noble metal Cd nanoparticles and CdS nanorods for efficient visible-light-driven photocatalytic H_2 evolution

Bo Wang[a], Sha He[a], Wenhui Feng[b], Lulu Zhang[a], Xueyan Huang[a], Kaiqiang Wang[a], Shiying Zhang[b], Ping Liu[a,*]

[a] Research Institute of Photocatalysis, State Key Laboratory of Photocatalysis on Energy and Environment, Fuzhou University, Fuzhou 350002, PR China
[b] Hunan Provincial Collaborative Innovation Center for Environment and Energy Photocatalysis, Changsha University, Changsha 410022, PR China

ARTICLE INFO

Keywords:
Cd/CdS nanocomposite
Non-noble metal
Morphology control
Photocatalytic H_2 evolution
Charge separation

ABSTRACT

Non-noble metal Cd nanoparticles, as an efficient cocatalyst, are successfully constructed onto the surface of hexagonal CdS nanorods (CdS NRs) for the photocatalytic hydrogen evolution reaction by a facile in situ chemical reduction approach based on a thermal treatment process. The in situ introduction of Cd can significantly improve the photocatalytic H_2 production performance of CdS NRs in sodium sulfide and sodium sulfite aqueous solutions under visible light irradiation. The superior electrical conductivity of metallic Cd and the intimate interfacial contact between Cd and CdS NRs are suggested to account for the enhanced light absorption intensity, more efficient charge separation, and faster interfacial charge migration, resulting in the dramatically promoted photocatalytic H_2 production activity. This work provides a new route for the in situ deposition of Cd nanoparticles onto CdS and other Cd-containing semiconductor photocatalysts with desired morphologies.

1. Introduction

Exploitation and utilization of environmental and renewable energy are very urgent for the worsening environmental problems and energy crisis. Photocatalytic hydrogen evolution from water is one of the most appealing processes to convert the inexhaustible water and solar power into clean and renewable energy [1–4]. This technology has attracted huge attention and becomes a hot topic during the past decades [5–7].

Various superior photocatalysts such as g-C_3N_4, CdS, TiO_2, and ZnS have been discovered for the photocatalytic hydrogen evolution to date [8–11]. Among them, CdS possesses a narrow band gap (Eg = 2.4 eV) and suitable band structure, making it the most popular photocatalyst for water splitting [12]. Unfortunately, the application of pristine CdS is mainly limited by rapid photoexciton recombination and the photocorrosion [13–15]. To improve the photocatalytic H_2 evolution efficiency, a great deal of strategies has been developed during the past decades, including semiconductor combination, metal modification, elements doping, surface sensitization, textural and crystal modification, etc. [16–20]. Among these strategies, metal cocatalysts were widely used as electron trap and active sites for promoting the photocatalytic H_2 evolution performance [21]. Generally, a Schottky junction can be built in the interface between metal nanoparticles and semiconductor photocatalysts, which would effectively promote the charge carriers separation, resulting in the significantly improved performance for photocatalytic H_2 evolution. Besides, to a certain extent, the photostability of photocatalysts can be improved by loading of metal cocatalysts [22]. Nonetheless, relevant studies focus on noble metals (such as Pt, Pd, and Ru), which are costly and scarce, the large-scale application of them is severely limited [23–25]. Hence, seeking economical and high-efficiency non-noble metal cocatalysts is of great urgency. Previous studies indicate that non-noble metals can play similar roles as the above noble metals [26,27]. For instance, we have reported a Bi/CdS nanocomposite with enhanced visible light photocatalytic performance, in which the non-noble metal Bi nanoparticles can indeed promote the charge carriers separation significantly [28]. However, the semiconductor heterostructure suffers from a serious lattice stress due to the different crystalline structures between metal Bi nanoparticles and CdS, exhibiting a limited improvement for charge carriers separation efficiency [29]. Thus, the continuity of crystalline structures in the interface would be the key of developing efficient photocatalysts in order to insure high-efficiency charge carriers transport.

As a non-noble metal with excellent electrical conductivity, Cd has attracted a great deal of interest recently [30,31]. Besides, metal Cd and

* Corresponding author.
E-mail address: liuping@fzu.edu.cn (P. Liu).

https://doi.org/10.1016/j.apcatb.2018.05.005
Received 1 February 2018; Received in revised form 27 April 2018; Accepted 2 May 2018
Available online 03 May 2018

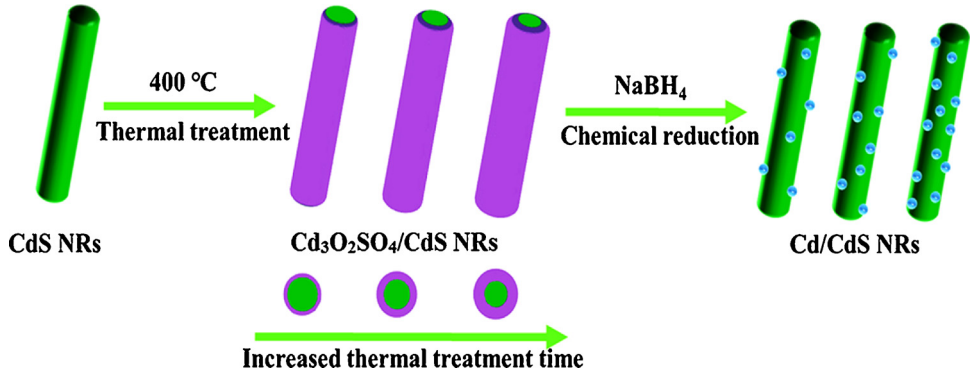

Scheme 1. Schematic synthesis process of the Cd/CdS NRs nanocomposites.

Cd-containing compounds possess the same element, cadmium. Thus, the integration of Cd and CdS with better lattice matching in the interface should be a potential visible light-driven composite photocatalyst. Actually, some relevant researches have been reported so far. Zhang et al. reported an oxidation-sulfurization route for the preparation of the CdS nanoparticle-decorated Cd nanosheets with an edge length of 1–3 μm and a thickness of 30-50 nm [32]. Nevertheless, the large-sized Cd nanosheets as cocatalysts cannot provide ample active sites for photocatalytic H_2 evolution due to their small specific surface area. Making the metal cocatalysts as small as possible is considered a useful way to provide more active sites. Therefore, Wang et al. prepared small sized Cd nanoparticles-decorated CdS by a photochemical method [33]. The nanocomposites exhibited dramatically improved photocatalytic activity. However, CdS substrates in this nanocomposite system show irregular in shape and agglomerated. Obviously, this route is difficult to control the morphology of CdS substrate and completely suppress carrier recombination. If one-dimensional (1D) shape such as nanorod is used instead of irregular shape, then 1D nanostructures could not only provide a short electron diffusion length perpendicular to their axis, but also transfer charge carriers quickly along the axis [34–37]. Those would result in a low carrier recombination in the 1D nanostructure and high photocatalytic efficiency. So we can fore that both high-efficiency interior and surface carriers separation may be obtained at the same time if we integrate the small sized Cd nanoparticles onto CdS with specific morphologies. Nevertheless, to our knowledge, the synthesis and application of this perfect photocatalyst have never been reported to date. Therefore, developing a facile and universal method to realize this promising structure model is significant.

In this work, we report an ingenious two-step in situ deposition method to construct Cd nanoparticle-decorated CdS NRs. This method can in situ assemble small sized Cd nanoparticles onto CdS substrates with desired morphologies, and don't change the original morphologies of them. In this route, the thermal treatment is seen as an essential procedure for the construction of the Cd/CdS NRs nanocomposites, which could adjust the surface and interface characteristics of CdS, thus the divalent Cd^{2+} species on the surface of CdS could be chemically reduced to Cd° easily. The content of metallic Cd would increase with the extension of thermal treatment time. An intimate interfacial contact is built between metallic Cd and CdS NRs, resulting in an efficient interfacial carriers separation. The optimal Cd/CdS NRs nanocomposite exhibits high hydrogen production performance under visible light irradiation ($\lambda > 410$ nm) due to the superior interior and interfacial carriers separation as well as the enhanced light absorption, the hydrogen evolution rate is about 16.1 times higher than that of pure CdS NRs. This work may provide an optimized model for constructing new Cd/CdS photocatalysts with high-efficiency interior and surface carriers separation. Furthermore, the facile in-situ deposition method is expected to be appropriate for other Cd-containing compounds to design rationally more efficient photocatalysts.

2. Experimental

2.1. Materials

Cadmium nitrate tetrahydrate ($Cd(NO_3)_2{\cdot}4H_2O$) was purchased from Aladdin Co. Ltd. (Shanghai, China). thiourea (CH_4N_2S), ethylenediamine ($C_2H_8N_2$), sodium borohydride ($NaBH_4$), ethanol (C_2H_6O), sodium sulfide nonahydrate ($Na_2S{\cdot}9H_2O$), and sodium sulfite (Na_2SO_3) were obtained from Sinopharm Chemical Reagent Co. Ltd. (Shanghai, China). All of the chemicals were analytical grade and used without further treatment. Deionized (DI) water was used throughout this study.

2.2. Synthesis of CdS NRs

CdS NRs were prepared by a solvothermal method. Typically, 5 *g* cadmium nitrate tetrahydrate and 3.7 *g* thiourea were dissolved in 60 mL ethylenediamine under continuous stirring to obtain a homogenous mixture. Then the obtained solution was stirred for about 1 h and transferred into a 100 mL Teflon-lined stainless steel autoclave. The autoclave was heated up to 180 °C and maintained for 24 h. After the autoclave cooled down to room temperature, the resulting precipitates were gathered by centrifugation and washed with absolute ethanol and deionized water for several times. Finally, the products were placed inside a vacuum oven and dried at 60 °C for 12 h.

2.3. Synthesis of Cd/CdS NRs composites

The Cd/CdS NRs photocatalyst was synthesized by an in situ chemical deposition method based on a thermal treatment process, the content of metallic Cd in Cd/CdS NRs composites could be adjusted by changing the thermal treatment time, as shown in Scheme 1. In this synthesis, 0.2 g CdS NRs was first placed into a muffle furnace and heated at 400 °C for an appropriate time with a heating rate of 5 °C/min. After cooling down to room temperature naturally, the resultant powders were dispersed into 50 mL 1 M $NaBH_4$ solution and stirred for about 4 h at room temperature. Subsequently, the resulting greenish products were filtered and washed with absolute ethanol and DI water for several times. Then the products were dried at room temperature overnight in vacuum oven. The CdS NRs heated for 1 h, 2 h, 3 h, 4 h, and 5 h under the same condition were labeled as Cd-CdS-1 h, Cd-CdS-2 h, Cd-CdS-3 h, Cd-CdS-4 h, and Cd-CdS-5 h, respectively.

2.4. Characterization

The crystal structure and purity of the as-prepared samples were identified by X-ray diffraction (XRD) patterns, which were carried out on a Bruker D8 ADVANCE X-ray diffractometer via $Cu_{K\alpha}$ radiation operated at 40 kV and 40 mA. The morphology and microstructure of the products were performed by field-emission scanning electron microscope (FESEM, HITACHISU8000) and transmission electron

microscope (TEM, Tecnai G2F20 S-TWIN, FEI Company) with a 200 kV accelerating voltage. A UV–vis diffuse reflectance spectroscopy monitored by a UV–vis-NIR spectrophotometer (Varian Cary-500) was utilized to investigate the optical properties of the samples, in which $BaSO_4$ was served as the reflectance standard. The photoluminescence (PL) spectra were collected using a FLS980 Series of Fluorescence Spectrometers with an excitation wavelength at 400 nm. A CHI660E electrochemical workstation with a conventional three-electrode system was used to record the photocurrents of the samples. Pt plate and Ag/AgCl electrode were used as counter and reference electrodes, respectively, and 0.1 M Na_2S and 0.1 M Na_2SO_3 aqueous solution was utilized as electrolyte. The electrochemical impedance spectroscopy (EIS) of the products was measured on a ZENNIUM electrochemical workstation (Zahner, Germany) in the presence of 10 mM $K_3[Fe(CN)_6]$/$K_4[Fe(CN)_6]$ and 0.5 M KCl aqueous solution, with the aforementioned three-electrode system. 5 mg of the product powder was dispersed into 0.5 mL N,N-dimethylformamide (DMF) solution under sonication for 1 h to obtain a homogenous slurry, and then 10 μL slurry was evenly spread on the surface of fluorine-doped tin oxide (FTO) glass substrate served as the working electrode with an area of 0.5 × 0.5 cm. After the as-obtained electrodes were dried at room temperature, the edge parts without coated samples of the electrodes were isolated by epoxy resin. The visible light source was a xenon lamp (300 W) with a cutoff filter ($\lambda > 410$ nm). Thermogravimetric analysis (TGA) was carried out with a STA449 C analyzer. The TGA curves were recorded in the temperature range of 50–650 ℃, at a heating rate of 5 ℃·min^{-1} in Air surrounding. X-ray photoelectron spectroscopy (XPS, Thermo ESCALAB 250XI) was utilized to explore the interaction of samples.

2.5. Photocatalytic activity measurements

The photocatalytic activities of the Cd nanoparticle-decorated CdS nanorods were evaluated by photocatalytic H_2 evolution reaction under visible light irradiation. In this photocatalytic measurement, 20 mg of as- prepared photocatalyst was dispersed into 100 mL mixed aqueous solution containing 0.1 M Na_2S and 0.1 M Na_2SO_3 under sonication, and then the suspension was migrated into a top-irradiation quartz reaction vessel. Subsequently, the reaction system was degassed by a vacuum pump for 1 h before irradiation to remove the residual air. The solution temperature was keep at 5 ℃ by a recirculated water cooling system. The above mentioned 300 W xenon lamp ($\lambda > 410$ nm) was used to vertically irradiate the suspension to produce hydrogen. The generated H_2 was detected every 1 h by a gas chromatograph (GC7900, Techcomp, Shanghai) coupled with a thermal conductivity detector, and Ar as the carrier gas.

3. Results and discussion

3.1. Phase structure and morphology

XRD patterns are conducted to analyze the crystal structure and purity of the as-prepared pure CdS NRs and series of Cd/CdS NRs nanocomposites. As shown in Fig. 1, the XRD pattern of pristine CdS NRs could be well indexed to hexagonal wurtzite structure with good crystallinity (JCPDS no. 41–1049, a = 4.14 Å and c = 6.72 Å). The essential crystal structure of the CdS NRs maintains well after the deposition of Cd nanoparticles. The new diffraction peaks at 31.84°, 34.75°, 38.37°, and 62.29° in the XRD patterns of Cd/CdS NRs composites could be assigned to the (002), (100), (101), and (110) lattice planes of metallic Cd (JCPDS no. 65-3363), respectively, indicating that part of the divalent Cd^{2+} species on the surface of CdS NRs is reduced to metallic Cd, and the predicted Cd/CdS nanorods are achieved. Actually, the approximate content of Cd in the Cd-CdS-4 h sample has been determined by TGA (as shown in Fig. S6). As estimated, the loading of Cd in Cd-CdS-4 h composite is about 1.77 wt%. With the thermal treatment time increasing, the corresponding diffraction peaks of metallic Cd become more intense, which demonstrates that the content of Cd nanoparticles could be adjusted by changing the thermal treatment time [28,33]. Besides, no trace of any impurities peaks is detected in the XRD patterns, indicating that Cd/CdS NRs photocatalysts with high purity are achieved. In order to demonstrate the proposed synthetic mechanism (as shown in Scheme 1), the XRD analysis of the thermal treated CdS NRs (labeled as $Cd_3O_2SO_4$-CdS-4 h) was carried out and shown in Fig. S1. It can be clearly seen that three new diffraction peaks corresponding to the $Cd_3O_2SO_4$ (JCPDS no. 26–0382) are observed [38]. Besides, the crystalline structure of CdS NRs doesn't change obviously after impregnation in $NaBH_4$ solution at the same condition as exhibited in Fig. S2. The corresponding sample is labeled as CdS NRs-$NaBH_4$. These consequences demonstrate that both of the thermal treatment and chemical reduction process are indispensable for the in situ deposition of Cd nanoparticles, and the proposed synthetic mechanism in this work is persuasive and well-grounded.

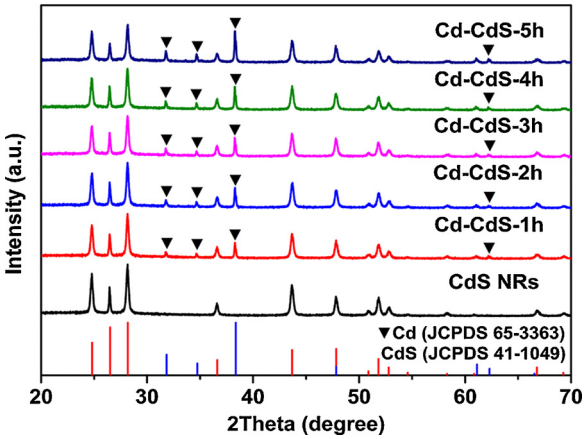

Fig. 1. Typical XRD patterns of the as-prepared bare CdS NRs and Cd/CdS NRs composites.

The microscopic morphology information of the pristine CdS NRs and Cd-CdS-4 h samples was investigated by SEM images. It can be seen in Fig. 2a, the pure CdS NRs has a rod shape with a diameter of 30–80 nm. No notable difference can be found after the deposition of Cd nanoparticles (as shown in Fig. 2 b). Although some nanoparticles are observed on the surface of Cd-CdS-4 h sample, these nanoparticles cannot be confirmed to be metallic Cd particles due to the similar atomic number contrast between metallic Cd and CdS [39]. TEM and HRTEM were performed to further certify the morphology and composition of the as-prepared Cd-CdS-4 h composite, and thus confirming the existence of metallic Cd nanoparticles in Cd-CdS-4 h sample. As presented in Fig. 2c, nanoparticles with size of about 30 nm have been successfully anchored on the surface of CdS nanorods. The HRTEM image of Cd-CdS-4 h sample (Fig. 2d) clearly shows two kinds of lattice fringes with fringe pacing of about 0.336 nm and 0.28 nm, which are consistent with the (002) lattice plane of hexagonal CdS and (002) crystal plane of metallic Cd, respectively [30]. These results clearly indicate that metallic Cd nanoparticles are indeed constructed onto the surface of CdS NRs successfully via the above-proposed in situ deposition method, which is accordant with the XRD data above.

3.2. Photocatalytic activity and stability

The photocatalytic performance of the prepared Cd/CdS NRs composites has been investigated by photocatalytic H_2 evolution reaction under visible light irradiation ($\lambda > 410$ nm). 0.1 M Na_2S and 0.1 M Na_2SO_3 mixed aqueous solutions are used as hole scavengers in the photocatalytic reaction system. As can be seen in Fig. 3, the pristine CdS nanorods exhibit a limited hydrogen evolution rate (0.16 mmol h^{-1} g^{-1}), which may be credited to the fast recombination

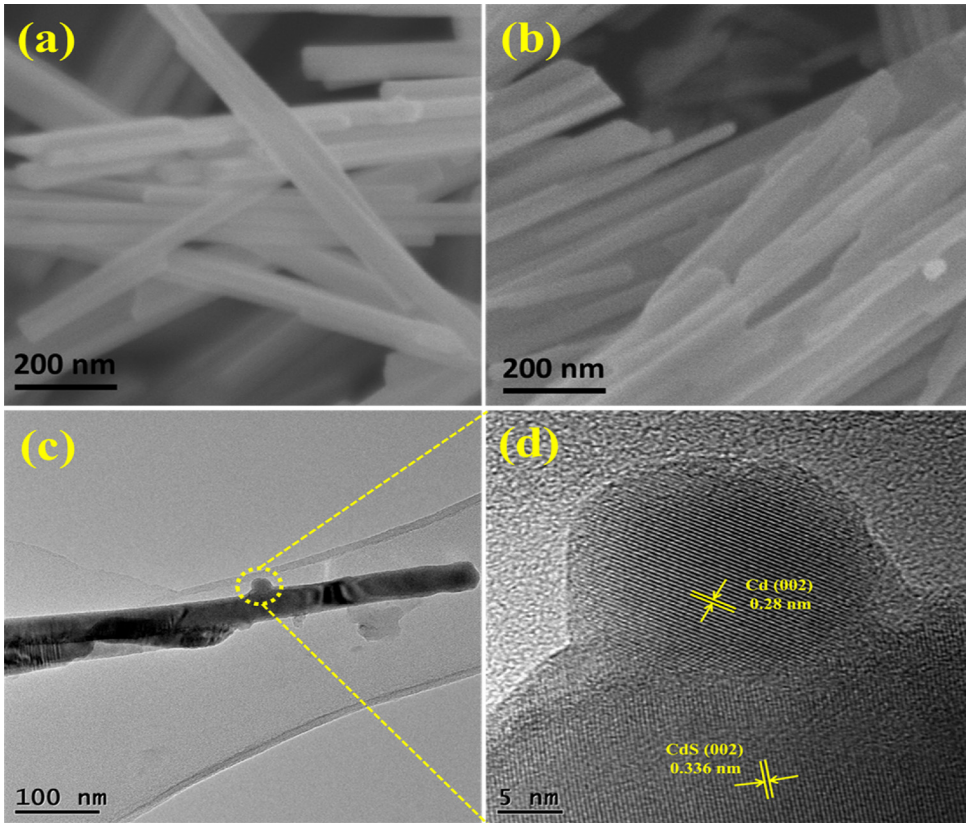

Fig. 2. SEM images of (a) pristine CdS NRs and (b) Cd-CdS-4 h composite; (c) TEM and (d) HRTEM images of Cd-CdS-4 h sample.

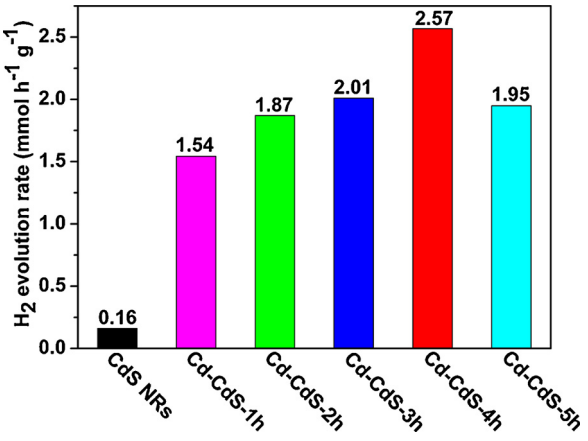

Fig. 3. Photocatalytic H_2 production rates of the prepared pure CdS NRs and Cd/CdS NRs composites.

of photoexcited electrons and holes. As prolonging thermal treatment time from 1 to 4 h for Cd-CdS-xh composites, the photocatalytic H_2 production rates increase significantly. The Cd-CdS-4 h sample exhibits the highest photocatalytic H_2 evolution rate (2.57 mmol h^{-1} g^{-1}), which is approximately 16.1 times higher than that of pure CdS nanorods. This value is also significantly higher than most of previous CdS-based photocatalysts (as shown in Table S1). Notably, the hydrogen evolution rate decreases sharply when the thermal treatment time further prolongs to 5 h. This phenomenon can be ascribed to the shielding effect of excessive Cd, which particles hinder the visible-light absorption of CdS NRs in the composites. Even so, the Cd-CdS-5 h sample still shows a more efficient photocatalytic H_2 evolution activity than that of pristine CdS NRs powders. This similar phenomenon has also been found in other previous researches for metal-semiconductor nanocomposites system [28,40–42]. In order to explore the influence of calcination temperature on activity, a series of Cd/CdS NRs are synthesized at different calcination temperatures, the H_2 evolution activity is carried out and shown in Fig. S7. Besides, for comparison, the photocatalytic activity of the thermal treated CdS NRs (labeled as $Cd_3O_2SO_4$-CdS-4 h) and $NaBH_4$ treated CdS NRs (labeled as CdS NRs-$NaBH_4$) was also executed under the same condition. The results have been shown in Fig. S3 and Fig. S4. It is clear that both $Cd_3O_2SO_4$-CdS-4 h and CdS NRs-$NaBH_4$ samples present unimproved hydrogen evolution rate compared with bare CdS NRs. These results demonstrate that Cd nanoparticles reduced by $NaBH_4$ based on a thermal treatment process are responsible for the enhanced photocatalytic performance.

It is well known that the stability of photocatalysts is another significant requirement for practical application. Therefore, the stability of the Cd-CdS-4 h composite is also investigated. Recycling experiment was executed on photocatalytic H_2 production activity and shown in Fig. 4a. It can be seen that no obvious decrease of H_2 production rate is observed after five consecutive runs without renewing the reagents and photocatalysts. Furthermore, XRD patterns and SEM images of Cd-CdS-4 h hybrid before and after five runs of photocatalytic H_2 evolution were recorded, and the results are shown in Fig. 4b and Fig. S5, respectively. As can be seen, both the crystal structure and morphology of Cd-CdS-4 h composite don't exhibit apparent change after photocatalytic reaction for 20 h. These results indicate that the prepared Cd/CdS NRs photocatalysts possess good stability during the photocatalytic reaction.

3.3. Optical properties and charge separation

In order to reveal the reasons for the improved photocatalytic H_2 production performance of the Cd/CdS NRs nanohybrids under visible light irradiation, UV–vis diffuse reflectance spectroscopy (DRS) was measured to investigate the optical performance of pure CdS NRs and

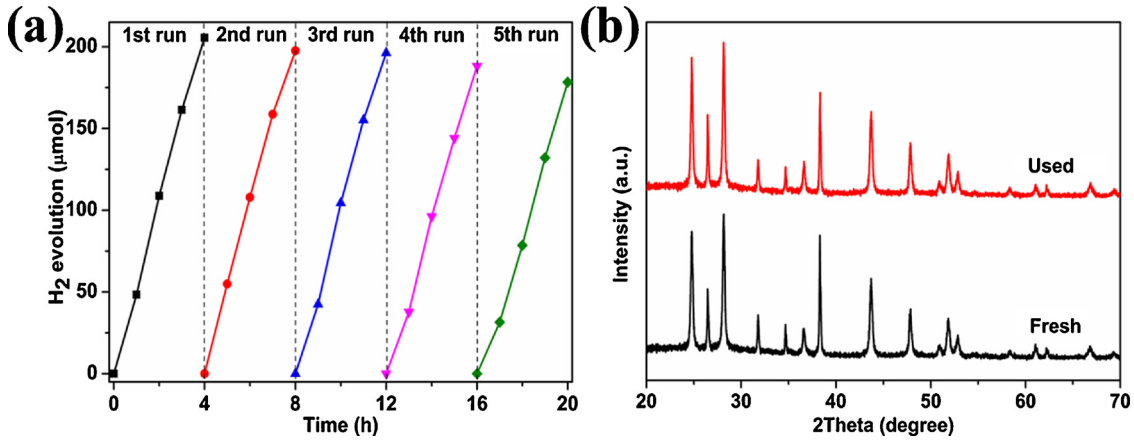

Fig. 4. (a) Time courses of photocatalytic H_2 evolution over Cd-CdS-4 h composite under visible light irradiation ($\lambda > 410$ nm); (b) XRD patterns of Cd-CdS-4 h before and after photocatalytic H_2 evolution reaction for 20 h under visible light irradiation.

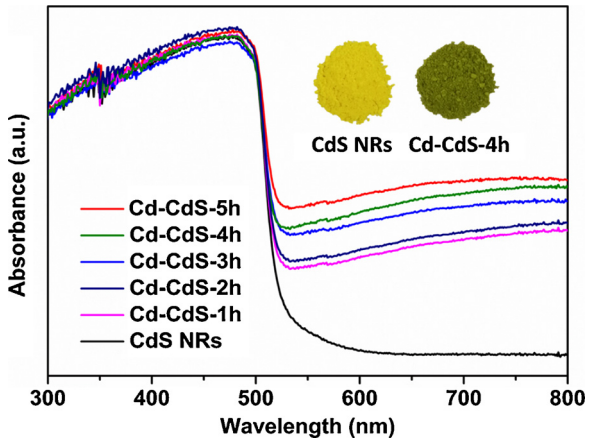

Fig. 5. UV–vis DRS patterns of the as-obtained pure CdS NRs and Cd/CdS NRs samples. Insert: the color of pristine CdS NRs and Cd-CdS-4 h composites.

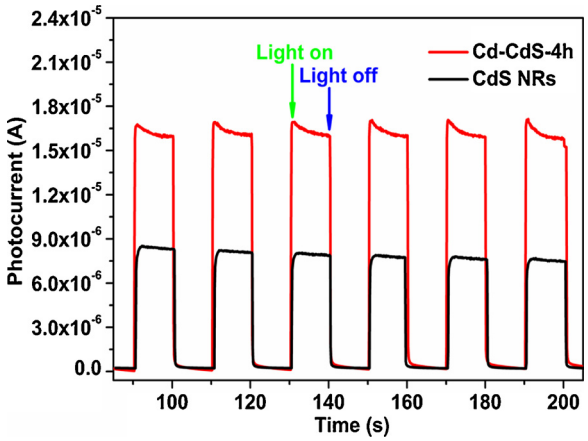

Fig. 6. Comparison of transient photocurrent responses of pristine CdS NRs and Cd-CdS-4 h.

Cd/CdS NRs nanocomposites. As displayed in Fig. 5, pristine CdS NRs and Cd/CdS NRs nanocomposites show the same absorption edge at 530 nm, which can be assigned to the intrinsic band gap absorption of CdS. Notably, a significant enhancement of absorption with the wavelength region of 530–800 nm can be detected after the deposition of Cd nanoparticles. The absorption in the visible light area for Cd/CdS NRs hybrids is gradually enhanced with prolonging time of thermal treatment process. Such absorption of Cd/CdS NRs hybrids is consistent with the color change sequence from yellow to green (as shown in inset of Fig. 5) induced by the black appearance of metallic Cd. These results suggest that the introduction of Cd nanoparticles could be responsible for the optimized optical property of Cd/CdS NRs samples, which may result in the improved photocatalytic H_2 evolution activity [33,43,56].

To understand the role of the deposited metallic Cd as electron trap, the transient photocurrent response with several light on-off cycles has been determined under visible light irradiation [44,57]. As shown in Fig. 6, the Cd-CdS-4 h photocatalyst exhibits a significantly higher photocurrent response than that of pristine CdS nanorods. It is known that the high photocurrent corresponds to a good photoinduced carrier separation [16,45,46]. Hence, the enhanced photocurrent of Cd-CdS-4 h means a more efficient separation, faster transmission or a longer lifetime of the photoexcited electron-hole pairs as compared to the CdS NRs. Electrochemical impedance spectroscopy (EIS) was also carried out to further research the interfacial charge transfer performance for pure CdS NRs and Cd-CdS-4 h sample [47–49]. As can be seen in Fig. 7, the Nyquist plot of the Cd-CdS-4 h sample shows a significant reduction in the radius of the semicycle arc as compared to pristine CdS nanorods,

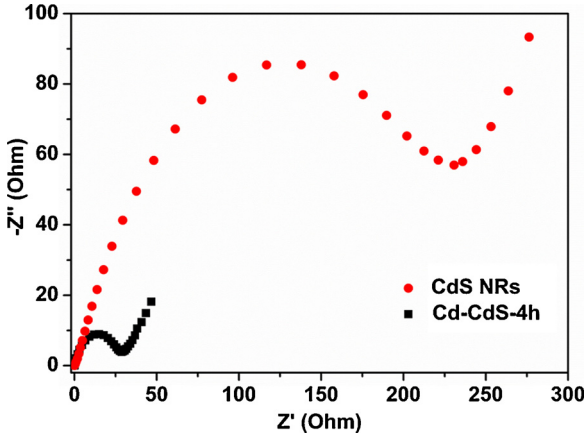

Fig. 7. EIS Nyquist plots of bare CdS NRs and the as-prepared Cd-CdS-4 h samples.

indicating a more efficient interfacial charge migration, which could owe the excellent electrical conductivity of metallic Cd and the intimate interface contact between metallic Cd and CdS nanorods. Furthermore, to further verify the conjecture that the in situ deposited metallic Cd can effectively facilitate the separation of the photogenerated charge carriers and inhibit their recombination, the photoluminescence (PL) emission spectra of Cd-CdS-4 h photocatalyst and bare CdS NRs were measured [50–52]. The excitation wavelength of the above

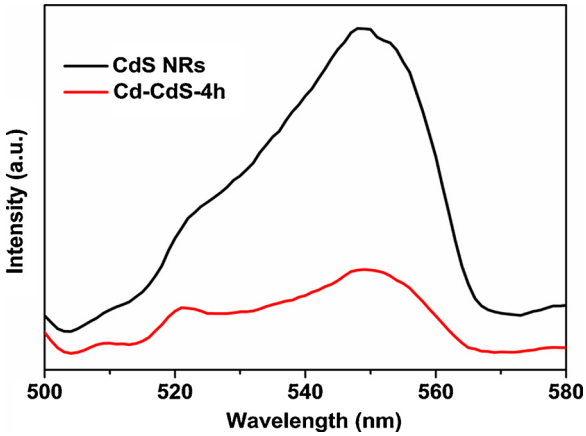

Fig. 8. PL emission spectra of pure CdS NRs and Cd-CdS-4 h.

measurements is 400 nm, and the results are shown in Fig. 8. The PL emission spectra exhibit two emission peaks centered at about 520 and 550 nm. The PL peak at 520 nm is ascribed to the essential excitonic emission of CdS NRs [39], which is in agreement with its band gap energy of 2.4 eV, while the peak at 550 nm is attributed to the deep trap emission related to the excess interface sulfur [53,54]. Cd-CdS-4 h shows a significantly decreased PL intensity as compared to bare CdS NRs, demonstrating that the Cd-CdS-4 h sample inhibits the photogenerated carrier recombination. These results correspond to the photocurrent data and EIS analysis above, which verify that the in situ deposited metallic Cd can effectively accelerate the separation and transmission of the photoexcited electrons and holes, and inhibit their recombination, and thus improve the photocatalytic performance of Cd/CdS NRs composites.

Furthermore, XPS is used to explore the interaction between Cd and CdS. As shown in Fig. S8, for the Cd 3d XPS spectra of the bare CdS sample, two strong peaks at 404.9 and 411.7 eV could be ascribed to Cd $3d_{5/2}$ and Cd $3d_{3/2}$ of Cd^{2+} in pure CdS NRs, respectively. By contrast, two new peaks at 404.4 and 411.2 eV can be detected in Cd-CdS-4 h composite, which could be assigned to Cd $3d_{5/2}$ and Cd $3d_{3/2}$ of Cd°, respectively. Notably, an obvious shift for about 0.3 eV toward higher binding energy can be observed in Cd 3d spectra after the in situ reduction of Cd. This shift indicates the existence of a strong interfacial interaction between Cd and CdS [55]. The intimate interfacial contact between metallic Cd and CdS nanorods can ensure fast migration of electrons from CdS to Cd, which results in enhanced H_2 evolution activity.

3.4. Photocatalytic mechanism

A feasible mechanism for the promoted photocatalytic H_2 evolution performance of the prepared Cd/CdS NRs photocatalysts could be illustrated in Scheme 2 based on the experimental results and analysis above. A Schottky junction can be formed in the interface between metallic Cd nanoparticles and CdS nanorods. Electrons are excited from the valence band (VB) to the conduction band (CB) of CdS NRs under visible light irradiation, leaving the holes in the VB. And then the electrons in the CB rapidly transfer to metallic Cd nanoparticles via the Schottky junction due to the excellent electrical conductivity of metallic Cd. Besides, the intimate interfacial contact between metallic Cd and CdS nanorods can ensure fast migration of electrons from CdS to Cd. Photoexcited electrons and holes are more difficult to recombine [58]. Thus, lifetimes of photogenerated electrons and holes are prolonged, which results in enhanced H_2 evolution activity. Then the electrons trapped by metallic Cd nanoparticles reduce H^+ into H_2, and the photogenerated holes in the VB of the CdS NRs oxidize the sacrificial reagents. As a substitute for noble metal, metallic Cd not only acts as an excellent electron trap but also can provide a large amount of hydrogen generation sites, which would significantly enhance the photocatalytic activity. Consequently, the Cd/CdS NRs nanocomposites show a superior photocatalytic H_2 evolution performance under visible light irradiation.

4. Conclusions

In summary, we have demonstrated an in situ chemical reduction method based on a thermal treatment process to synthesize metallic Cd nanoparticles modified CdS nanorods. The in situ deposited metallic Cd significantly improves the photocatalytic H_2 production performance of CdS NRs via this route. The content of metallic Cd would increase with the extension of thermal treatment time. The optimal thermal treatment time is determined to be 4 h, and the resulting Cd-CdS-4 h sample exhibits the highest H_2 production activity and superior stability. The dramatically improved photocatalytic H_2 evolution performance of Cd/CdS NRs can be ascribed to the enhanced light absorption intensity, more efficient charge separation, and faster interfacial charge migration due to the in situ deposition of Cd with superior electrical conductivity. In addition, a probable mechanism for the promoted photocatalytic performance is proposed. The above experimental results demonstrate the non-noble metal Cd can be used as a promising cocatalyst for the construction of economical and efficient Schottky junction photocatalysts. It is expected that this facile in situ deposition approach could offer a new inspiration for rational design and exploration of Cd/CdS

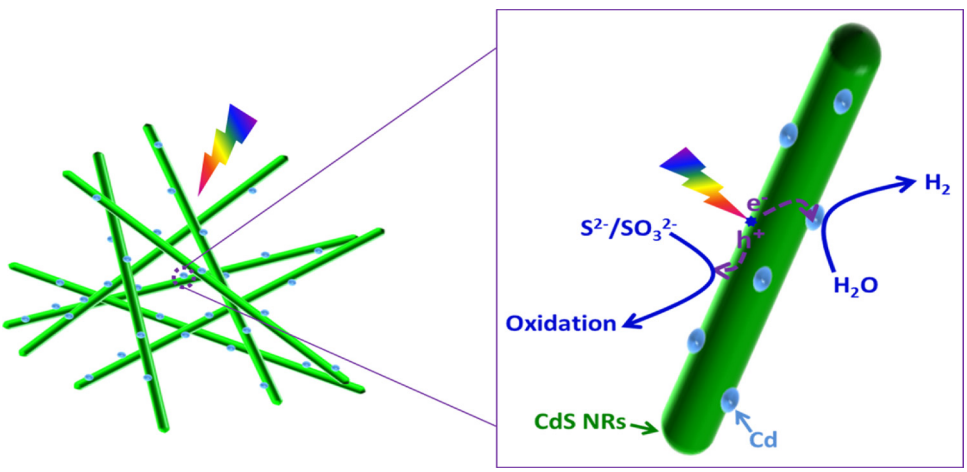

Scheme 2. Schematic illustration of the proposed mechanism for the photoinduced carriers migration for photocatalytic H_2 evolution over the Cd/CdS NRs photocatalysts under visible light irradiation.

and other Cd-modified Cd-containing semiconductor nanohybrids with high-efficiency carriers separation in interior and on surface.

Acknowledgements

This work is supported by the National Natural Science Foundation of China (21473031, 21673041), and the National Key Technologies R & D Program of China (2014BAC13B03).

Appendix A. Supplementary data

Supplementary material related to this article can be found, in the online version, at doi: https://doi.org/10.1016/j.apcatb.2018.05.005.

References

[1] J. Ran, J. Zhang, J. Yu, M. Jaroniec, S.Z. Qiao, Chem. Soc. Rev. 43 (2014) 7787–7812.
[2] A. Kudo, Y. Miseki, Chem. Soc. Rev. 38 (2009) 253–278.
[3] X. Zou, Y. Zhang, Chem. Soc. Rev. 44 (2015) 5148–5180.
[4] K. Takanabe, ACS Catal. 7 (2017) 8006–8022.
[5] Q. Wang, T. Hisatomi, Y. Suzuki, Z. Pan, J. Seo, M. Katayama, T. Minegishi, H. Nishiyama, T. Takata, K. Seki, A. Kudo, T. Yamada, K. Domen, J. Am. Chem. Soc. 139 (2017) 1675–1683.
[6] T.F. Yeh, S.J. Chen, H. Teng, Nano Energy 12 (2015) 476–485.
[7] Q. Wang, T. Hisatomi, Q. Jia, H. Tokudome, M. Zhong, C. Wang, Z. Pan, T. Takata, M. Nakabayashi, N. Shibata, Y. Li, I.D. Sharp, A. Kudo, T. Yamada, K. Domen, Nat. Mater. 15 (2016) 611–615.
[8] G. Zhang, M. Zhang, X. Ye, X. Qiu, S. Lin, X. Wang, Adv. Mater. 26 (2014) 805–809.
[9] Q. Li, B. Guo, J. Yu, J. Ran, B. Zhang, H. Yan, J.R. Gong, J. Am. Chem. Soc. 133 (2011) 10878–10884.
[10] Q. Xiang, J. Yu, M. Jaroniec, J. Am. Chem. Soc. 134 (2012) 6575–6578.
[11] J. Zhang, Y. Wang, J. Zhang, Z. Lin, F. Huang, J. Yu, ACS Appl. Mater. Interfaces 5 (2013) 1031–1037.
[12] M. Luo, W. Yao, C. Huang, Q. Wu, Q. Xu, J. Mater. Chem. A 3 (2015) 13884–13891.
[13] X. Wang, K. Maeda, X. Chen, K. Takanabe, K. Domen, Y. Hou, X. Fu, M. Antonietti, J. Am. Chem. Soc. 131 (2009) 1680–1681.
[14] W. Zhang, Y. Wang, Z. Wang, Z. Zhong, R. Xu, Chem. Commun. 46 (2010) 7631–7633.
[15] F. Ma, Y. Wu, Y. Shao, Y. Zhong, J. Lv, X. Hao, Nano Energy 27 (2016) 466–474.
[16] J. Zhang, Y. Wang, J. Jin, J. Zhang, Z. Lin, F. Huang, J. Yu, ACS Appl. Mater. Interfaces 5 (2013) 10317–10324.
[17] O. Rosseler, C. Ulhaq-Bouillet, A. Bonnefont, S. Pronkin, E. Savinova, A. Louvet, V. Keller, N. Keller, Appl. Catal. B: Environ. (166-167) (2015) 381–392.
[18] S. Cho, J.W. Jang, J.S. Lee, K.H. Lee, Crystengcomm 12 (2010) 3929–3935.
[19] S. Weng, Z. Pei, Z. Zheng, J. Hu, P. Liu, ACS Appl. Mater. Interfaces 5 (2013) 12380–12386.
[20] J. Chen, F. Qiu, W. Xu, S. Cao, H. Zhu, Appl. Catal. A: Gen. 495 (2015) 131–140.
[21] H. Li, H. Yu, L. Sun, J. Zhai, X. Han, Nanoscale 7 (2015) 1610–1615.
[22] W. Choi, G. Park, K.-L. Bae, J.Y. Choi, K.M. Nam, H. Song, J. Mater. Chemistry A 4 (2016) 13414–13418.
[23] K. Wu, Z. Chen, H. Lv, H. Zhu, C.L. Hill, T. Lian, J. Am. Chem. Soc. 136 (2014) 7708–7716.
[24] M. Luo, P. Lu, W. Yao, C. Huang, Q. Xu, Q. Wu, Y. Kuwahara, H. Yamashita, ACS Appl. Mater. Interfaces 8 (2016) 20667–20674.
[25] Y.J. Zhang, L. Zhang, Appl. Surf. Sci. 255 (2009) 4863–4866.
[26] G. Han, Y.H. Jin, R.A. Burgess, N.E. Dickenson, X.M. Cao, Y. Sun, J. Am. Chem. Soc. 139 (2017) 15584–15587.
[27] W.J. Foo, C. Zhang, G.W. Ho, Nanoscale 5 (2013) 759–764.
[28] B. Wang, W. Feng, L. Zhang, Y. Zhang, X. Huang, Z. Fang, P. Liu, Appl. Catal. B: Environ. 206 (2017) 510–519.
[29] W. Feng, Y. Wang, X. Huang, K. Wang, F. Gao, Y. Zhao, B. Wang, L. Zhang, P. Liu, Appl. Catal. B: Environ. 220 (2018) 324–336.
[30] J. Zhao, C. Ye, X. Fang, Y. Peng, Z. Wang, L. Zhang, J. Cryst. Growth 277 (2005) 445–449.
[31] W.S. Khan, C. Cao, T. Mahmood, M. Ahmad, F.K. Butt, Z. Ali, Z. Usman, F. Wang, Q.U. Ain, Mater. Lett. 65 (2011) 1896–1899.
[32] L. Shang, B. Tong, H. Yu, G.I.N. Waterhouse, C. Zhou, Y. Zhao, M. Tahir, L.-Z. Wu, C.-H. Tung, T. Zhang, Adv. Energy Mater. 6 (2016) 1501241.
[33] Q. Wang, J. Li, Y. Bai, J. Lian, H. Huang, Z. Li, Z. Lei, W. Shangguan, Green. Chem. 16 (2014) 2728–2735.
[34] S. Liu, Z.R. Tang, Y. Sun, J.C. Colmenares, Y.J. Xu, Chem. Soc. Rev. 44 (2015) 5053–5075.
[35] J.L. Xie, C.X. Guo, C.M. Li, Energy Environ. Sci. 7 (2014) 2559–2579.
[36] Z. Han, G. Chen, C. Li, Y. Yu, Y. Zhou, J. Mater. Chem. A 3 (2014) 1696–1702.
[37] B. Weng, S. Liu, N. Zhang, Z.R. Tang, Y.J. Xu, J. Catal. 309 (2014) 146–155.
[38] Y. Fan, M. Deng, G. Chen, Q. Zhang, Y. Luo, D. Li, Q. Meng, J. Alloys Compd. 509 (2011) 1477–1481.
[39] X. Fu, L. Zhang, L. Liu, H. Li, S. Meng, X. Ye, S. Chen, J. Mater. Chem. A 5 (2017) 15287–15293.
[40] Y. Zhang, H. Fan, M. Li, H. Tian, Dalton Trans. 42 (2013) 13172–13178.
[41] X. Bai, R. Zong, C. Li, D. Liu, Y. Liu, Y. Zhu, Appl. Catal. B: Environ. 147 (2014) 82–91.
[42] C. Wang, Y. Ao, P. Wang, J. Hou, J. Qian, S. Zhang, Mater. Lett. 64 (2010) 439–441.
[43] G. Yang, W. Yan, Q. Zhang, S. Shen, S. Ding, Nanoscale 5 (2013) 12432–12439.
[44] L. Zhang, W. Feng, B. Wang, K. Wang, F. Gao, Y. Zhao, P. Liu, Appl. Catal. B: Environ. 212 (2017) 80–88.
[45] J. Jin, J. Yu, D. Guo, C. Cui, W. Ho, Small 11 (2015) 5262–5271.
[46] Y. Lv, Y. Liu, Y. Zhu, Y. Zhu, J. Mater. Chem. A 2 (2013) 1174–1182.
[47] G. Li, Z. Lian, W. Wang, D. Zhang, H. Li, Nano Energy 19 (2016) 446–454.
[48] B. Cao, G. Li, H. Li, Appl. Catal. B: Environ. 194 (2016) 42–49.
[49] Y. Liu, W. Yao, L. Di, R. Zong, Z. Mo, X. Ma, Y. Zhu, Appl. Catal. B: Environ. 163 (2015) 547–553.
[50] Z. Zhao, W. Zhang, Y. Sun, J. Yu, Y. Zhang, H. Wang, F. Dong, Z. Wu, J. Phys. Chem. C 120 (2016) 11889–11898.
[51] Y. Huo, X. Yang, J. Zhu, H. Li, Appl. Catal. B: Environ. 106 (2011) 69–75.
[52] S. Chen, Y. Hu, S. Meng, X. Fu, Appl. Catal. B Environ. (150–151) (2014) 564–573.
[53] Y. Wang, G. Meng, L. Zhang, A. Changhao Liang, J. Zhang, Chem. Mater. 14 (2002) 1773–1777.
[54] H. Park, Y.K. Kim, W. Choi, J. Phys. Chem. C 115 (2011) 6141–6148.
[55] K. Cheng, W. Sun, H.-Y. Jiang, J. Liu, J. Lin, J. Phys. Chem. C 117 (2013) 14600–14607.
[56] M. Xing, W. Xu, C. Dong, Y. Bai, J. Zeng, Y. Zhou, J. Zhang, Y. Yin, Chem (2018), http://dx.doi.org/10.1016/j.chempr.2018.03.002.
[57] C. Dong, C. Lian, S. Hu, Z. Deng, J. Gong, M. Li, H. Liu, M. Xing, J. Zhang, Nat. Commun. 9 (2018) 1252.
[58] Y. Wang, X. Zhao, D. Cao, Y. Wang, Y. Zhu, Appl. Catal. B: Environ. 211 (2017) 79–88.